Nuclear Magnetic Resonance Chemical Shifts and Quadrupole Couplings for Different Hydrogen-Bonding Cases Occurring in Liquid Water: A Computational Study

Teemu S. Pennanen,*,† Perttu Lantto,‡ Atte J. Sillanpää,§ and Juha Vaara‡

NMR Research Group, Department of Physical Sciences, P.O. Box 3000, FIN-90014 University of Oulu, Finland, Laboratory of Physical Chemistry, Department of Chemistry, P.O. Box 55 (A. I. Virtasen aukio 1), FIN-00014 University of Helsinki, Finland, and CSC - Scientific Computing Ltd., P.O. Box 405, FI-02101 Espoo, Finland

Received: August 25, 2006; In Final Form: October 12, 2006

Nuclear magnetic resonance (NMR) parameters are determined theoretically for the oxygen and hydrogen/deuterium nuclei of differently hydrogen-bonded water molecules in liquid water at 300 K. The parameters are the chemical shift, the shielding anisotropy, the asymmetry parameter of shielding, the nuclear quadrupole coupling constant, and the asymmetry parameter of the nuclear quadrupole coupling. We sample instantaneous configurations from a Car−Parrinello molecular dynamics simulation and feed nuclear coordinates into a quantum chemical program for the calculation of NMR parameters using density-functional theory with the three-parameter hybrid exchange-correlation (B3LYP) functional. In the subsequent analysis, molecules are divided into groups according to the number of hydrogen bonds they possess, and the full average NMR tensors are calculated separately for each group. The classification of the hydrogen-bonding cases is performed using a simple distance-based criterion. The analysis reveals in detail how the NMR tensors evolve as the environment changes gradually from gas to liquid upon increasing the number of hydrogen bonds to the molecule of interest. Liquid-state distributions of the instantaneous values of the NMR properties show a wide range of values for each hydrogen-bonding species with significant overlap between the different cases. Our study shows how local changes in the environment, along with classical thermal averaging, affect the NMR parameters in liquid water. For example, a broken or alternatively extra hydrogen bond induces major changes in the NMR tensors, and the effect is more pronounced for hydrogen or deuterium than for oxygen. The data sheds light on the usefulness of NMR experiments in investigating the local coordination of liquid water.

1. Introduction

Solvent shifts of nuclear magnetic resonance (NMR) parameters can be approached in a variety of ways.[1] The environment around the solute may be modeled by a dielectric continuum or by using a supermolecular model, i.e., by surrounding the molecule of interest by explicit solvent molecules. Continuum models used alone have been shown to fail to describe many important contributions to the solvent shifts of NMR parameters.[2−4] Thus, these models can only be used alongside other methods to accommodate long-range electrostatic effects. In the supermolecular approach, one can use either finite-size clusters[3,5] or infinite periodic structures.[6,7] Finite-size clusters can be constructed according to chemical intuition, they may be optimized to produce minimum-energy structures, or they can be chosen as snapshots from a simulation trajectory. Clusters may then be fed into a quantum chemical program for the calculation of NMR parameters.[3] Infinite structures are produced by periodically replicating a finite-size unit cell obtained on-the-fly in a first-principles molecular dynamics (MD) simulation,[8] and then followed by a calculation of the NMR parameters using a procedure appropriate to periodic systems.[6,7]

Recently, we carried out a first-principles computational study on the nuclear shielding and quadrupole coupling (NQC) tensors of liquid water.[9] For the first time, the anisotropic properties of the tensors were also systematically calculated in the liquid state, using the Eckart axis system[10,11] to represent the tensors in a well-defined frame common to all instantaneous geometries of the solvated molecule. The calculation took advantage of a Car−Parrinello MD (CPMD) simulation[8] of a liquid sample of 32 water molecules, followed by Hartree−Fock and density-functional theory (DFT) calculations of the shielding and NQC tensors for clusters extracted from the simulation. In the previous paper,[9] property averages were reported for the whole sample of randomly chosen snapshots, disregarding any information that would refer to different instantaneous local hydrogen-bonding situations.

The local structure of liquid water has recently been subjected to a lot of interest. The interpretation of the X-ray data by Wernet et al.[12] has challenged the usual picture of a dynamic hydrogen-bonding network in which the molecules form slightly less than four hydrogen bonds on average. According to ref 12, a 2-fold coordination, with one hydrogen-bond acceptor and one donor, is the dominating local structure, suggesting that water molecules tend to form rings and chains in the liquid state. This interpretation of the X-ray data has been questioned by several groups,[13,14] and comments are being exchanged back and forth.[15,16]

* Corresponding author. E-mail: teemu.pennanen@oulu.fi.
† University of Oulu.
‡ University of Helsinki.
§ CSC Scientific Computing.

10.1021/jp065507w CCC: $37.00
Published on Web 12/14/2006

NMR is considered to be a sensitive probe of the local structure of the sample around the resonating nuclei.[17] Against this background, it is natural to inquire whether NMR experiments would also be able to shed light on the question of the average number of hydrogen bonds in liquid water. This would be likely if the NMR parameters of differently hydrogen-bonded water molecules were systematically different. Klein, Mennucci, and Tomasi[18] have studied optimized cluster geometries and found a monotonic decrease in the ^{17}O shielding constant as the number of hydrogen bonds is increased from zero to four. They mentioned also that for molecules having three hydrogen bonds small systematic differences in the ^{17}O shielding constant were found depending on whether the hydrogen bond is missing from the oxygen side or from the hydrogen side. Also, Cybulski and Sadlej[19] studied optimized water clusters and found similar dependencies of the ^{17}O shielding constant on the cluster size. One may assume that a prerequisite for the existence of an applicable experimental NMR procedure for the local structure of liquid water is that the distributions of the parameters within the different species are relatively well separated.

In the present article, we subject the previously obtained[9] MD trajectory of liquid water and the computed NMR data into an analysis in which the statistical sample is divided into smaller groups, each containing only the snapshots in which the central molecule has *n* hydrogen bonds, where *n* is an integer in the range of 2 to 6. Here we call these groups hydrogen-bonding species. The criterion used in the division into different species is a matter of choice. Presently we employ a simple distance-based cutoff between the oxygen and hydrogen nuclei of the hydrogen-bond acceptor and donor molecules, respectively. This procedure provides a chance to investigate the change in the NMR parameters caused by different local structures in the first coordination shell. The results are also indicative of the environmental effects on the NMR parameters (due to other water molecules) when only a partial filling of the first coordination shell occurs, for example, in confined geometries at interfaces, in apolar solutions, or in porous materials.

2. Theory and Computational Details

The basic theory of NMR parameters relevant to this work is described in our previous article[9] and is not repeated here. Moreover, the details of the simulations, the quantum-chemical NMR calculations, the sampling of the trajectory, and the estimation of statistical errors are covered there at length. Here we limit ourselves to a quick review of the relevant information.

Two CPMD simulations,[20] one for the liquid and the other for the gaseous state, were carried out for the isotopomer $^1H_2{}^{16}O$ using classical dynamics for the atomic nuclei. The liquid simulation contained 32 molecules in a cubic box with all sides equal to 18.62 au, producing a density of 1.000 g cm^{-3}. The gas-phase simulation contained one molecule in a cubic box with sides equal to 12.2 au. Both simulations used DFT with the BLYP[21] exchange-correlation functional, Vanderbilt pseudopotentials for both oxygen and hydrogen,[22] and a plane-wave cutoff energy of 24 Ry. The time step in integrating the equations of motion was 0.12 fs, and the fictitious mass parameter for the electrons was $\mu = 600$ au. The simulations were performed in the microcanonical *NVE* ensemble without constraints, with the temperature fluctuating around 300 K. The lengths of the thermalization and production phases were about 1.2 and 3 ps for the liquid, respectively, and about 4 and 5 ps for the gas, respectively.

Four hundred roughly spherical clusters cut out from the liquid-state trajectory, and the same number of single-molecule configurations from the gas simulation, were used as an input for quantum-chemical calculations of nuclear magnetic shielding (σ) and NQC (χ) tensors using the Dalton code[23] performed with the DFT/B3LYP[24] method. For shielding constants, DFT/B3LYP has been shown to perform well in general[25−28] and gives an acceptable description for water, as shown in the recent paper by Cybulski and Sadlej.[19] A carefully chosen[9] locally dense basis set was used with the aug-cc-pVDZ[29] basis on the central molecule and approximations thereof for the nearest neighbors and for molecules in the second solvation shell. The clusters contained 10−20 molecules (15 on average), and they were placed in a spherical cavity cut into a dielectric continuum[30] to take care of long-range electrostatic effects.

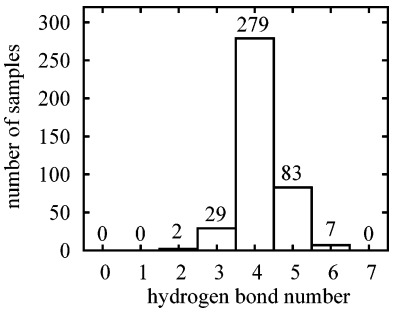

Figure 1. Hydrogen bond distribution in the liquid state at 300 K, as obtained from 400 randomly chosen clusters from a Car−Parrinello molecular dynamics simulation.

Intramolecular motion and intermolecular interactions affect molecular properties, making them dependent on the instantaneous configuration. A molecule in the liquid state experiences different hydrogen-bonding situations over time, and the values of a certain parameter can span a large interval. Even in the gas phase, where there are practically no neighboring molecules, the rovibrations of the molecule cause significant changes in the parameters.

To identify the hydrogen bonds in the clusters, one needs a criterion for a hydrogen bond to exist. Usually, such criteria are based on the pair-interaction energy between two molecules or on the intermolecular distances and angles for certain nuclei. Here, the former case is called the energy criterion,[31,32] and the latter is called the distance criterion.[33,34] The hydrogen-bond criterion used in this work is a simple one-parameter distance criterion. A pair of water molecules has a hydrogen bond if the intermolecular OH distance is less than or equal to 2.72 Å, the sum of the van der Waals radii of the hydrogen (1.20 Å) and oxygen (1.52 Å) atoms. A comparison of our choice with the strong hydrogen bond definition of Mezei and Beveridge[33] shows that the maximum OH distances are the same within 1%.

3. Results and Discussion

3.1. Hydrogen Bond Distribution. Our hydrogen bond criterion leads to the hydrogen bond distribution shown in Figure 1. The most probable configuration is the one with four neighbors hydrogen bonded to the central molecule. The next highest probability is for 5-fold hydrogen-bonding, in which an extra acceptor or donor falls within our hydrogen-bonding criterion. The number of these subcases is 25 for the occurrence of an extra acceptor (species *5a*) and 58 for an extra donor (species *5d*). The third significant species is with three H-bonds in which either one acceptor (species *3a*, 6 cases) or one donor (species *3d*, 23 cases) molecule is missing. The rest of the molecules form either six or two hydrogen bonds, but these species are not present in significant numbers. It can also be seen that the overall average number of hydrogen bonds is

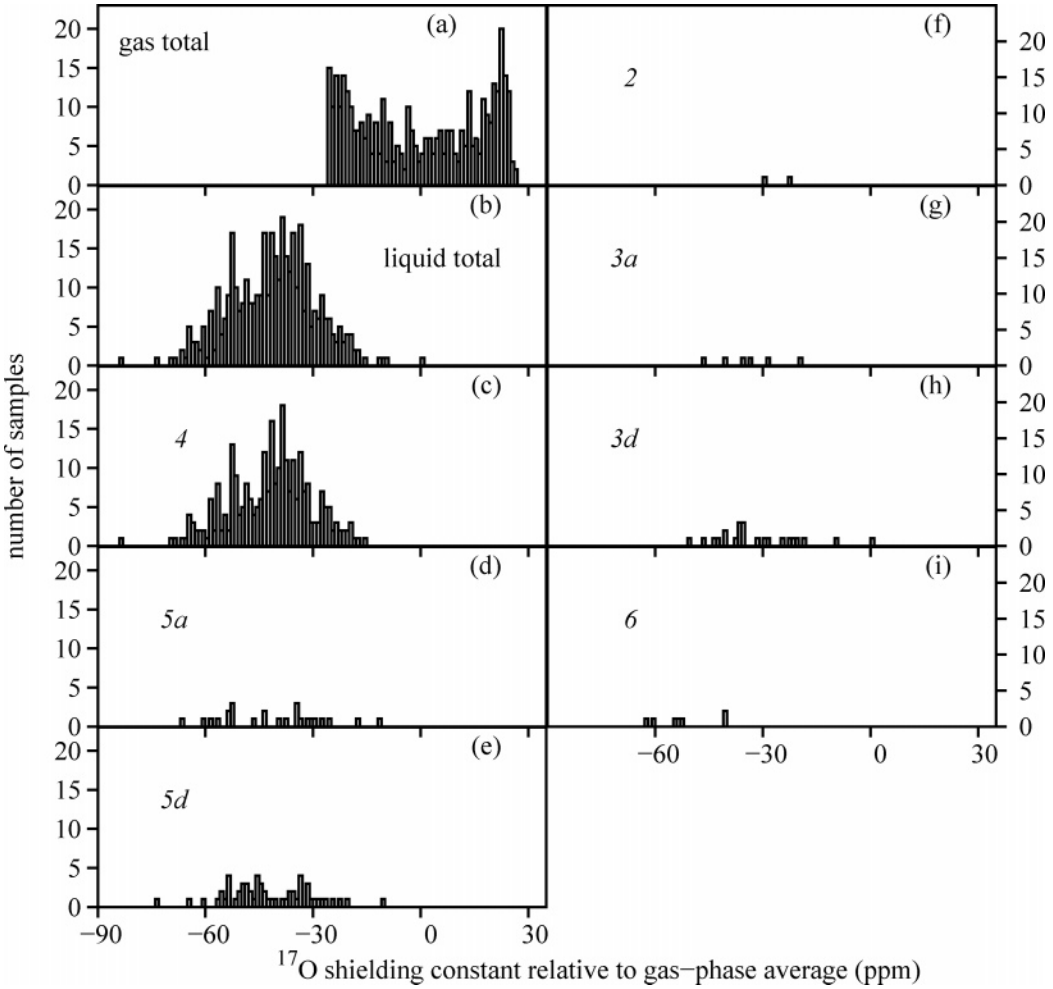

Figure 2. Distributions of the isotropic ^{17}O shielding constant for liquid and gaseous water at 300 K, broken down into the various hydrogen-bonding species. (a) Total distribution for gas, (b) total distribution for liquid, (c) liquid molecules with four hydrogen bonds (HBs), (d) five HBs, with an extra hydrogen-bond acceptor (*5a*), (e) five HBs, with an extra hydrogen-bond donor (*5d*), (f) two HBs, (g) three HBs, acceptor missing (*3a*), (h) three HBs, donor missing (*3d*), and (i) six HBs.

slightly larger than four. This reflects both the underlying CPMD trajectory and our limited sampling thereof and needs not be of great concern here because the hydrogen bond distribution is not the major goal of this study. Instead, we focus on the trends of the average parameters as functions of the number of hydrogen bonds and on the distributions of the parameters within each species. However, varying the hydrogen bond criterion evidently changes the hydrogen bond distribution. As the distance criterion is decreased from 2.72 Å, the distribution shifts toward smaller hydrogen bond numbers. Most noticeably, the number of the species having three H-bonds increases at the expense of species having five H-bonds. In this way, the average number of hydrogen bonds could in principle be adjusted.

3.2. Property Value Distributions of the Hydrogen-Bonding Species.

3.2.1. Shielding Constant Distributions for ^{17}O. Figure 2 shows the distributions of the isotropic ^{17}O nuclear shielding constant for each hydrogen-bonding species, along with the total distributions in the gaseous and liquid states. The distributions have been placed on a scale in which the average of the gas-phase distribution is set to zero. We see that the distributions in the gaseous and liquid states differ significantly. Their overall shapes are different, and the centers of gravity of the distributions are displaced. This displacement is identified as the gas-to-liquid shift. It is −41.2 ppm for our sample at the B3LYP level,[9] whereas the experimental shift is −36.1 ppm.[35,36]

The double-peak shape of the gaseous distribution is reminiscent of the position distribution of the classical harmonic oscillator. This finding can be rationalized qualitatively as follows. The two stretching vibrations of the water molecule, the symmetric and asymmetric stretches, are mainly responsible for the variation of the oxygen shielding constant. The bending mode is less significant because the ^{17}O shielding is not very sensitive to the angular variation.[11] The effect of the two bond lengths on the oxygen shielding may be considered pairwise additive to a first approximation. The two stretching modes of the molecule have certain relative weights that are dictated by the initial configuration. Ideally, the relative weights remain constant for a harmonically vibrating molecule without any interaction with the surroundings. In fact, because the ^{17}O shielding constant in water is roughly linearly dependent on the deviation of one bond length from the equilibrium value,[11] the asymmetric mode in which the two hydrogens move in opposite directions with respect to the equilibrium value and thus have opposite effects contributes very little to the ^{17}O shielding constant. In contrast, in the symmetric stretch the two bond lengths change in phase and affect the ^{17}O shielding in the same direction. The position distribution in the symmetric stretching mode is that of a classical harmonic oscillator, and thus the overall ^{17}O shielding distribution resembles the position distribution of the classical harmonic oscillator. A true gas-phase molecule undergoes collisions that modify the relative weights

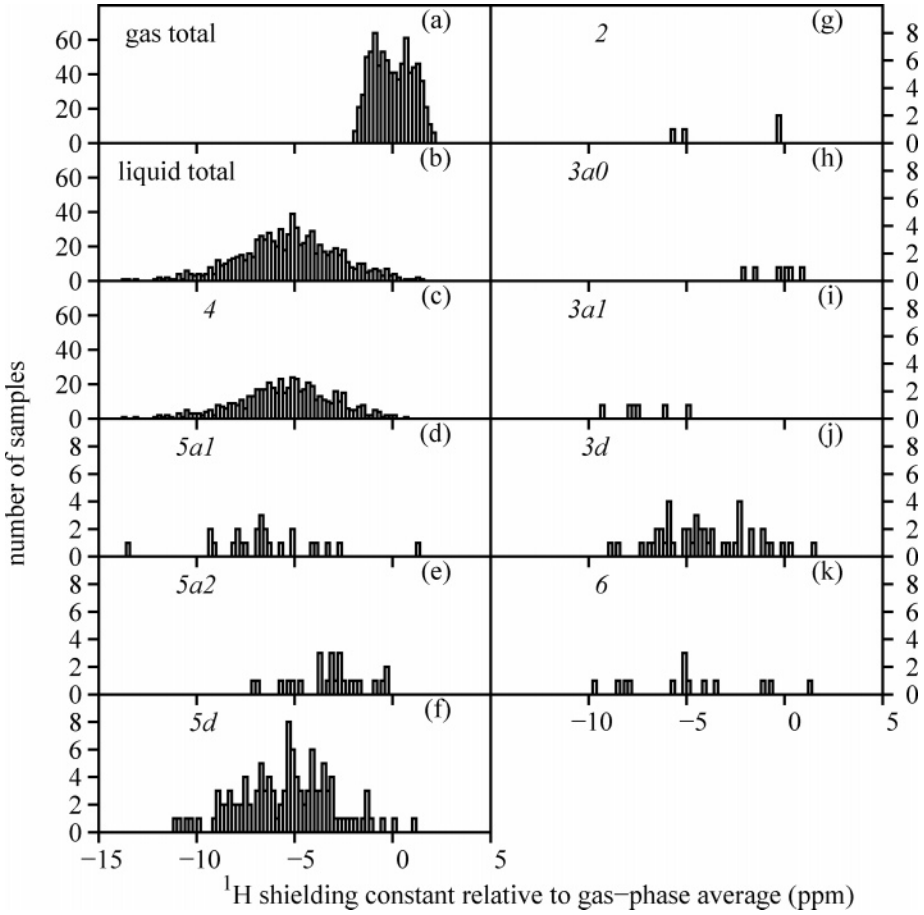

Figure 3. As in Figure 2 but for the isotropic ^{1}H shielding constant. (a) Total distribution for gas, (b) total distribution for liquid, (c) liquid molecules with four hydrogen bonds (HBs), (d) five HBs, with the resonating proton having a bond with one acceptor oxygen (*5a1*), (e) five HBs, with the resonating proton having a bond with two acceptor oxygens (*5a2*), (f) five HBs, with an extra hydrogen bond donor (*5d*), (g) two HBs, (h) three HBs, acceptor oxygen missing from the resonating proton (*3a0*), (i) three HBs, with the resonating proton having a bond with an acceptor oxygen (*3a1*), (j) three HBs, with one hydrogen bond donor missing (*3d*), and (k) six HBs. Notice the change in the vertical scale in panels d−k.

of the stretching modes. However, because the asymmetric stretch has little effect anyway, the ^{17}O shielding distribution always has a shape similar to that of Figure 2a.

In the liquid-state distribution in panel b, however, the presence of the neighboring molecules disturbs the oscillations. The stochastic nature of these interactions causes the shape of the distribution to be Gaussian. The width of the gas-phase distribution is around 53 ppm, whereas the tails of the liquid-state distribution extend to a range spanning more than 60 ppm.

The distribution of species with four H-bonds (species *4*) in panel c is very similar to the overall liquid distribution because the former constitutes almost 70% of the latter. The shapes of the other distributions are not clearly revealed because the number of samples belonging to those hydrogen-bonding species is small. However, it can be seen that their centers of gravity vary from the high values of the 2-fold hydrogen-bonded cases (in which the minute sample size naturally causes the position of the distribution to be only weakly hinted at) to the slightly lower values for *3a* and *3d*, further down to the *4*, *5a*, and *5d* cases, whose distributions all fall in the same range, and finally to the very low values of the 6-fold hydrogen-bonded case. A decreasing trend in the shielding constant may be expected with an increasing number of closest neighbors in an instantaneous configuration. This is connected with a higher density of virtual electronic states available for the negative, second-order paramagnetic part of nuclear shielding through which to operate. The widths of the distributions are substantial in practically all cases, causing the distributions of differently hydrogen-bonded species to overlap significantly.

3.2.2. Shielding Constant Distributions for ^{1}H. The number of samples in the ^{1}H property distributions is twice the number of ^{17}O samples because each hydrogen nucleus is considered to be a separate sample. Figure 3 illustrates the distribution of isotropic ^{1}H shielding constants in the gas and liquid phases and for the different hydrogen-bonding species in the liquid.

Similarly to the case of ^{17}O shielding, we have moved the origin of the shielding scale to the average of the gas-phase distribution. This time there are additional panels in the figure as compared to the case of ^{17}O because in the species *3* and *5* the two hydrogens in the same molecule are not equivalent with respect to the local environment. In the 3-fold hydrogen-bonded case, either a hydrogen-bond donor is missing for the investigated molecule (*3d*) or an acceptor is missing. In the latter case, the hydrogen without the hydrogen bond is called *3a0*, whereas the other hydrogen with the hydrogen bond is called *3a1*. In the 5-fold hydrogen-bonded configurations, the molecule of interest may be hydrogen bonded to three donors (*5d*), or one of its hydrogen atoms participates in hydrogen bonding with two acceptor molecules. From the point of view of the NMR parameters of the hydrogen nucleus, the latter instances are further categorized into ones in which the NMR nucleus is hydrogen bonded to only one (*5a1*) or two (*5a2*) acceptors.

The distribution of the instantaneous values of the ^{1}H shielding constant displays some evidence of the double-peak

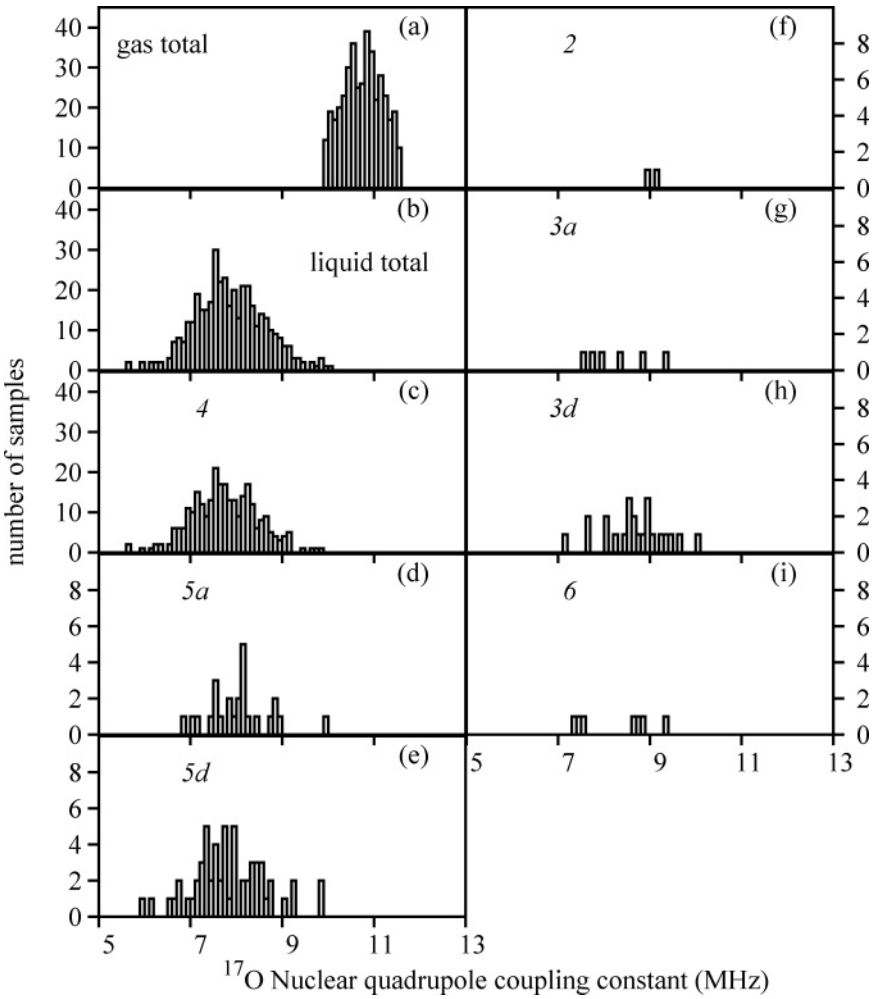

Figure 4. Distributions of the ^{17}O nuclear quadrupole coupling constant for liquid and gaseous water, and for various hydrogen-bonding species occurring in the liquid at 300 K. Please refer to Figure 2 for explanations of panels a−i. Notice the change in the vertical scale in panels d−i.

character in the gaseous state. The liquid-state distribution is Gaussian and is much wider than the gaseous distribution. This is in contrast to the corresponding distributions for the ^{17}O shielding constant. The liquid-state distribution appears to be similar to the distribution found by Sebastiani and Parrinello.[37] The gas-to-liquid shift is found to be −5.26 ppm,[9] the experimental shift being −4.26 ppm.[38,39] Similarly to the case of ^{17}O shielding, the distribution of the 4-fold hydrogen-bonded configurations closely resembles the total liquid distribution.

When the resonating proton has no nearby oxygen with which to form a hydrogen bond (species *3a0*), its shielding constant is close to the gaseous value, as seen in panel h. This may be expected on the basis of reduced paramagnetic contributions in this case, as discussed above. The *3a1* case with the resonating proton hydrogen bonded to an acceptor (panel i) displays the opposite effect, with much lower shielding than the average of the total liquid-state distribution. The two distributions are well separated on the shielding scale, with no overlap in the present, limited statistical sample. The case of 3-fold hydrogen-bonding with a missing donor (*3d*, panel j) is intermediate to the *3a0* and *3a1* cases.

In the 5-fold hydrogen-bonded configurations, when the hydrogen of interest has two neighbors close enough to form hydrogen bonds according to our distance criterion (species *5a2*, panel e), the shift is again close to the gaseous-state value. From the simulation data, it is seen that in the *5a2* species the two hydrogen-bonded oxygens are most often quite far from the central hydrogen and thus have a relatively small effect on ^{1}H shielding. However, there are some configurations within species *5a2* in which the central hydrogen has one short hydrogen bond that is accompanied by the other oxygen much further away but is still within the hydrogen-bonding distance. In this case, the more distant oxygen has only a minor effect on ^{1}H shielding. As mentioned earlier, decreasing the distance criterion for hydrogen bonding potentially changes the species to which individual clusters belong. For example, some clusters in the *5a2* species (according to the current criterion) with one short and one long hydrogen bond could turn into species *4* by losing the long bond. Similarly, the *5a2* cluster with two long bonds could turn into *3a0* by losing both of them.

An opposite effect on the shielding constant is seen for the hydrogen having one hydrogen-bonded acceptor in the *5a1* configuration (panel d) in which the average shift is larger than that for the liquid state in total. These hydrogens participate in a strong hydrogen bond. Similarly to the *3d* instances, the *5d* configurations, in which the molecule of interest is hydrogen bonded to three donors simultaneously, are intermediate between the extremes represented by the *3a1*/*5a1* cases on one hand and the *3a0*/*5a2* cases on the other in their ^{1}H shielding constants. However, in contrast to the well-separated *3a0* and *3a1* distributions, the *5a1* and *5a2* configurations display a significant overlap in their ^{1}H shielding constant distribution.

The number of hydrogen bond donors bonded to the center oxygen also has an effect on hydrogen shielding. A difference of well over 1 ppm is found between the *3d* (panel j) and *5d* (panel f) instances, having three and five neighbors, respectively.

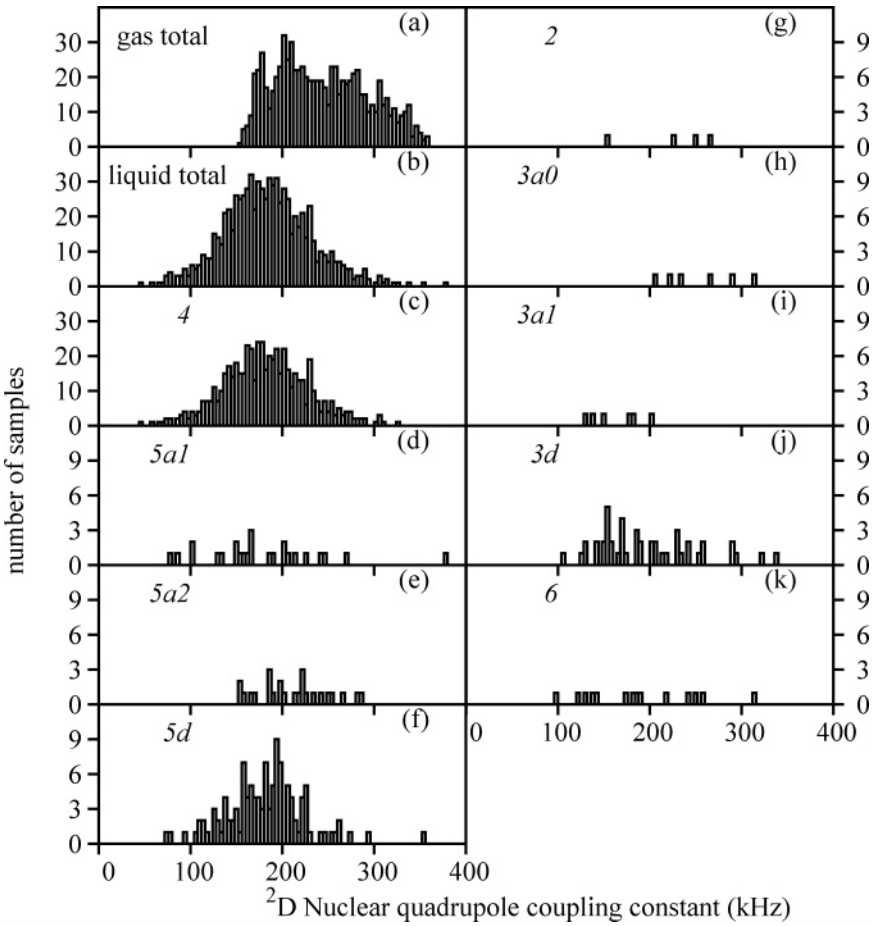

Figure 5. Distributions of the ^{2}D nuclear quadrupole coupling constant for liquid and gaseous water and for various hydrogen-bonding species occurring in the liquid at 300 K. Please refer to Figure 3 for explanations of panels a−k. Notice the change in the vertical scale in panels d−k.

In the latter case, the distribution is somewhat wider as well. The few samples within species *6* are widely distributed, owing to the possibility of having substantially different hydrogen-bonding patterns in this case. The very limited sample of 2-fold hydrogen-bonded configurations (with both one donor and one acceptor missing) is divided into cases where the resonating proton has or does not have a hydrogen bond to an acceptor. The two cases expectedly have low and high ^{1}H shielding constants, in the respective order.

3.2.3. Nuclear Quadrupole Coupling Distributions for ^{17}O and ^{2}D. The distributions of ^{17}O and ^{2}D NQCCs are visualized in Figures 4 and 5, respectively. There is no sign of double-peak character in the gaseous distribution of the nuclear quadrupole coupling constants (NQCCs) of either oxygen or deuterium. Because other premises are exactly the same as in the case of shielding constants, this implies that the dependence of the ^{17}O or ^{2}D NQCC on the bond length contains significant nonlinearity, as is known from the literature for ^{2}D.[40] Whereas the gas-phase distribution of ^{17}O NQCC is quite narrow and well separated from the liquid-state distribution at lower values, the corresponding gas-phase ^{2}D distribution is wide and skewed with significant overlap with the liquid-state distribution. For both nuclei, the dominance of the 4-fold hydrogen-bonded configurations is reflected in the close correspondence of the NQCC distribution with that of the total liquid. For ^{17}O NQCC, the distributions corresponding to many species fall practically superimposed on each other. This reflects the similar hydrogen-bonding situation with two donors bonded to the NMR nucleus. The exceptions include species *2* and *3d* in panels f and h, respectively, in which the oxygen only has one hydrogen-bonded neighbor. This causes the corresponding averages to reside closer to the gaseous value.

Referring to the gas-phase situation, the first hydrogen bond donor is seen to lower the ^{17}O NQCC roughly by 2 MHz, whereas the further effect of adding another one, to reach the above-mentioned "normal" local situation with two donors, is a decrease of about 1 MHz. Adding the third donor upon entering the *5d* species has only a minor further lowering effect on the ^{17}O NQCC. The successive displacements from the *3a* distribution (acceptor missing) to the distribution of species *4* (acceptor added) and further to the distribution of *5a* (another acceptor added) are about −0.4 and +0.3 MHz, respectively, with the *3d* configurations situated closest to the gas-phase range of values. This indicates that ^{17}O NQCC is also sensitive to the presence of the hydrogen-bond acceptors, albeit the effect of the latter is not as large as that of the donors that are close to the ^{17}O nucleus.

For ^{2}D NQCC, species *3a0* and *5a2* are the most gas like; exactly as was found for the ^{1}H shielding constants. Again, this is due to the long average hydrogen-bonding distances for the two nearby oxygens of the *5a2* hydrogen and the fact that the *3a0* hydrogen has no nearby neighbors. The *3a1* instances, with the resonating nucleus having a hydrogen-bond have, expectedly, the center of gravity of their ^{2}D NQCC distribution well in the liquid-like range. In parallel with the behavior of the *3a0* and *3a1* distributions of ^{1}H shielding, also the ^{2}D NQCC distributions are well separated for these configurations.

3.3. Property Averages for Hydrogen-Bonding Species. The averages of the shielding and NQCC distributions for the

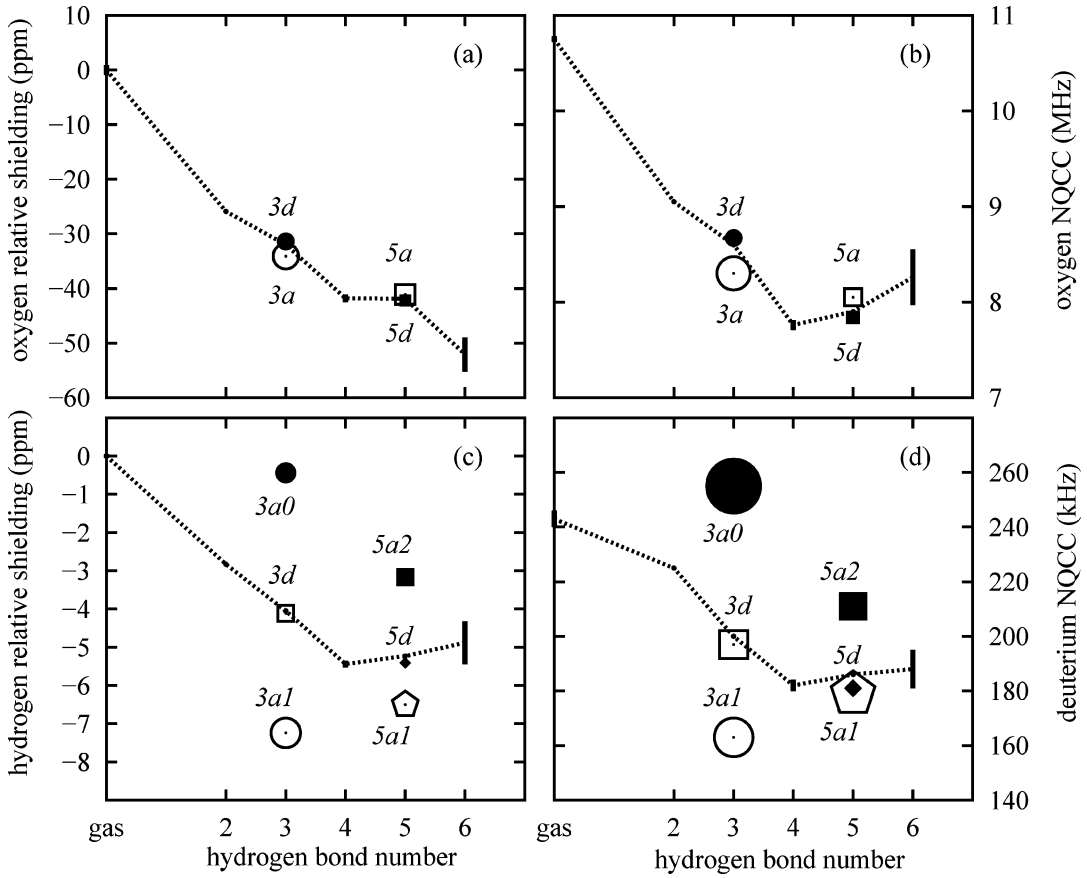

Figure 6. Average shielding and quadrupole coupling constants of the differently hydrogen-bonded water molecules in liquid water at 300 K. (a) ^{17}O shielding and (b) ^{17}O NQCC, with symbols as follows: ○, *3a;* ●, *3d*; □, *5a*; ■, *5d.* (c) ^{1}H shielding and (d) ^{2}D NQCC, with symbols as follows: ○, *3a1*; ●, *3a0*; □, *3d*; ⌂, *5a1;* ■, *5a2;* ♦, *5d.* The symbol sizes represent the error limits. For the notation of the different hydrogen-bonding species, please refer to Figures 2 and 3. The error limits for gaseous species and species *4* and *6* are displayed as vertical thick lines. For species *2*, the error limits have been omitted because of the small size of the statistical sample. Dashed lines go through the average values within species *2*−*6* without further classification into subcategories.

TABLE 1: ^{17}O Nuclear Shielding Constants, Shielding Tensor Anisotropies, Asymmetry Parameters, and Nuclear Quadrupole Coupling Constants and the Corresponding Asymmetry Parameters for Differently Hydrogen-Bonded Water Molecules in Liquid Water at 300 K[a]

gas	*2*	*3a*	*3d*	*4*	*5a*	*5d*	*6*	liquid
				oxygen shielding constant σ (ppm)				
309.7 (±0.9)	283.8	276 (±4)	278 (±3)	267.9 (±0.7)	269 (±3)	268 (±2)	258 (±4)	268.5 (±0.6)
				oxygen shielding anisotropy $\Delta\sigma^b$ (ppm)				
48.0 (±0.2)	35.7	31 (±5)	44.1 (±1.5)	32.6 (±0.7)	37 (±2)	31.2 (±1.3)	34 (±4)	33.3 (±0.6)
				oxygen shielding asymmetry parameter η^b				
0.037 (±0.002)	0.079	0.050 (±0.011)	0.049 (±0.007)	0.028 (±0.002)	0.032 (±0.007)	0.031 (±0.004)	0.031 (±0.011)	0.029 (±0.002)
				oxygen nuclear quadrupole coupling constant χ^b (MHz)				
10.75 (±0.03)	9.05	8.1 (±0.3)	8.61 (±0.14)	7.66 (±0.05)	7.93 (±0.14)	7.78 (±0.11)	8.2 (±0.3)	7.77 (±0.04)
				oxygen nuclear quadrupole coupling constant asymmetry parameter η^b				
0.652 (±0.007)	0.724	0.81 (±0.04)	0.74 (±0.04)	0.800 (±0.009)	0.77 (±0.03)	0.76 (±0.02)	0.73 (±0.07)	0.786 (±0.007)

[a] The error limits are in parentheses. See Figure 2 for the specification of the hydrogen-bonding species. The error limits for species *2* have not been included because of the very limited statistical sample size. [b] Obtained by diagonalization of the average tensor. $\Delta\sigma = \sigma_{33} - {}^1/_2(\sigma_{22} + \sigma_{11})$ and $\eta = (\sigma_{22} - \sigma_{11})/\sigma_{33}$, where the σ_{ii} are the eigenvalues of the average shielding tensor ordered as $\sigma_{33} > \sigma_{22} > \sigma_{11}$. $\chi = \chi_{33}$ is the largest eigenvalue of the average quadrupole coupling tensor, and the corresponding asymmetry parameter is defined as $\eta = |(\chi_{22} - \chi_{11})/\chi_{33}|$, where the χ_{ii} are the eigenvalues of the average tensor ordered as $|\chi_{33}| > |\chi_{22}| > |\chi_{11}|$.

various hydrogen-bonding species are displayed in Figure 6 and listed in Tables 1 and 2. The Tables also contain the data for shielding anisotropy and the asymmetry parameters of both shielding and NQC. For both nuclei, both shielding constants and NQCCs decrease monotonically from the gas-phase situation with no hydrogen-bonding partners to the 2-, 3-, and 4-fold

TABLE 2: ^{1}H Nuclear Shielding Constants, Shielding Tensor Anisotropies, Asymmetry Parameters, and ^{2}D Nuclear Quadrupole Coupling Constants and the Corresponding Asymmetry Parameters for Differently Hydrogen-Bonded Water Molecules in Liquid Water at 300 K[a]

gas	*2*	*3a1/3a0*	*3d*	*4*	*5a1/5a2*	*5d*	*6*	liquid
hydrogen shielding constant σ (ppm)								
30.07 (±0.05)	27.24	22.8/29.6 (±0.6/±0.5)	26.0 (±0.4)	24.63 (±0.09)	23.6/26.9 (±0.6/±0.4)	24.7 (±0.3)	25.2 (±0.6)	24.80 (±0.08)
hydrogen shielding anisotropy $\Delta\sigma$ (ppm)								
16.08 (±0.08)	21.8	30/15.2 (±3/±0.7)	24.3 (±0.7)	26.1 (±0.2)	29.1/20.0 (±1.1/±0.8)	26.1 (±0.5)	22.5 (±1.0)	25.7 (±0.2)
hydrogen shielding asymmetry parameter η								
0.0494 (±0.0006)	0.027	0.065/0.07 (±0.006/±0.02)	0.055 (±0.007)	0.0324 (±0.0014)	0.046/0.070 (±0.007/±0.008)	0.028 (±0.003)	0.031 (±0.007)	0.0347 (±0.0013)
deuterium nuclear quadrupole coupling constant χ (kHz)								
243 (±3)	224	163/254 (±11/±16)	197 (±8)	182 (±2)	178/211 (±13/±8)	181 (±5)	188 (±7)	184 (±2)
deuterium nuclear quadrupole coupling constant asymmetry parameter η								
0.1498 (±0.0009)	0.152	0.164/0.108 (±0.015/±0.009)	0.144 (±0.006)	0.135 (±0.002)	0.141/0.118 (±0.008/±0.006)	0.141 (±0.004)	0.118 (±0.006)	0.1353 (±0.0014)

[a] The error limits are in parentheses. See the footnotes to Table 1.

hydrogen-bonded cases. After the 4-fold species, the trend is stopped, and the average 5-fold instances have approximately the same shieldings and NQCCs as do the 4-fold cases.

In the upper-left panel of Figure 6, crowding in the environment with six neighbors increases the oxygen chemical shift beyond the average liquid level. The ^{17}O shifts of the *3a*/*3d* species differ only a little from each other, as do those for the *5a*/*5d* species. Cases *3d* and *5a* with fewer hydrogen bond donors always have properties closer to the gas-phase values than those of the *3a* and *5d* cases in which there are more neighboring molecules hydrogen bonded to the oxygen nucleus. This holds both for ^{17}O shielding constants and for NQCCs. These results can be compared with those found by Klein et al.[18] using a cluster approach with a varying number of neighbors at optimized geometries: As the number of hydrogen bonds is increased from zero to four, a monotonic decrease of the ^{17}O shielding constant is observed. They also found small, systematic differences between ^{17}O shielding constants of the *3a* and *3d* species.

For the hydrogen shielding constant in Figure 6c, the vicinity of the neighboring oxygen of a hydrogen bond acceptor has a huge effect on the chemical shift: when the hydrogen does not participate in a hydrogen bond (*3a0* instances), the shielding and NQCC are very close to the gaseous value, as noticed earlier. On the contrary, in the *3a1* instances in which the hydrogen in question is hydrogen bonded to an acceptor, the chemical shift and the change in the NQCC are much larger than the shift or coupling difference (from the gas-phase value) in the 4-fold hydrogen-bonded cases. It thus appears that the proximity of oxygen atoms of acceptor molecules to both hydrogens balances the hydrogen shift in the 4-fold hydrogen-bonded cases and beyond.

The *3d* configurations fall into a decreasing trend that displays the average value of each of species *2*, *3*, *4*, *5*, and *6* without further classification into subcategories. The difference of the *3d* results and those for the 4-fold species reveals that the ^{1}H shielding and ^{2}D NQCC are also sensitive to the coordination of the oxygen nucleus in the same molecule. Whereas the ^{1}H shielding and ^{2}D NQCC of the *5d* configuration with an extra hydrogen-bond donor are very similar to those in the species *4*, the *5a1* configuration deviates a bit further away from the gas-phase results, and the *5a2* configuration again displays the effect of two rather long hydrogen bonds, with results much closer to the gas-phase values.

For the hydrogen/deuterium in the gas phase and liquid state and for species *3d*, *4*, *5d*, and *6*, the error limits are calculated by first taking the average value of the property for the two equivalent nuclei in the same molecule, followed by averaging over the species in question and computing the error limit as the standard deviation of the mean value in the latter averaging. For species *3a0*, *3a1*, *5a1*, and *5a2* with the nonequivalent hydrogen/deuterium nuclei, the error limit is the standard deviation of the mean value when averaging over the species in question. For species *2*, the error limits have been omitted because of the small size of the statistical sample.

3.4. Full Average Tensors of Hydrogen-Bonding Species. *3.4.1. Shielding Tensors for ^{17}O and ^{1}H.* Figures 7 and 8 show the full average shielding tensors for the different hydrogen-bonding species for ^{17}O and ^{1}H nuclei, respectively. The tensors are the averages of the instantaneous shielding tensors expressed in an Eckart coordinate frame[10] chosen to coincide with the principal axis system of the moment of inertia tensor of the H_2O molecule at rest. The common frame of reference for each instantaneous configuration enables a component-wise summation of the individual tensors to form an average tensor.[9] In this frame, the molecule is in the *xy* plane, with the C_2 axis in the *y* direction.

The average gas- and liquid-state ^{17}O shielding tensors are diagonal, at least to within doubled error limits. This need not be the case, however, for the various hydrogen-bonding species where the oxygen nucleus in general does not have C_{2v} site symmetry. The tensor of species *4* closely resembles the total liquid tensor. All of the diagonal ^{17}O shielding tensor components feature a decreasing trend with an increase in the number of hydrogen bonded neighbors. In particular, the *xx* component (in the plane of the molecule, perpendicular to the C_2 symmetry axis) is rather sensitive to the details of the environment. In the *3d* configuration, the resonating ^{17}O nucleus has a "hole" in its local coordination shell, hence the σ_{xx} component is close to the locally similar 2-fold hydrogen-bonded case. The *5a* instances with crowded hydrogen-bond acceptors also feature a slight deviation from the decreasing trend.

The 2-fold hydrogen-bonded configurations have large off-diagonal components particularly in-plane (*xy* and *yx*) and between the direction of the C_2 axis and the normal to the molecular plane (*yz* and *zy*). The variety of local environments in the 6-fold hydrogen-bonded species is reflected in the large error limits of the tensor components. One can confirm that the

$$\boldsymbol{\sigma}_{^{17}\mathrm{O}}^{\mathrm{B3LYP}}(g) = \begin{pmatrix} 341.7 \pm 1.0 & 0.0 \pm 0.5 & 0.0 \pm 0.0 \\ 0.0 \pm 0.4 & 300.0 \pm 0.9 & 0.0 \pm 0.0 \\ 0.0 \pm 0.0 & 0.0 \pm 0.0 & 287.5 \pm 0.9 \end{pmatrix}$$

$$\boldsymbol{\sigma}_{^{17}\mathrm{O}}^{\mathrm{B3LYP}}(2) = \begin{pmatrix} 306.1 & -7.7 & -0.4 \\ -4.6 & 278.0 & 14.3 \\ -0.5 & 8.8 & 267.3 \end{pmatrix}$$

$$\boldsymbol{\sigma}_{^{17}\mathrm{O}}^{\mathrm{B3LYP}}(3a) = \begin{pmatrix} 295 \pm 5 & -5 \pm 5 & -4 \pm 4 \\ -3 \pm 4 & 273 \pm 5 & 2 \pm 3 \\ -1 \pm 2 & 2 \pm 2 & 258 \pm 5 \end{pmatrix}$$

$$\boldsymbol{\sigma}_{^{17}\mathrm{O}}^{\mathrm{B3LYP}}(3d) = \begin{pmatrix} 308 \pm 3 & -3 \pm 3 & -2.4 \pm 1.1 \\ 3 \pm 3 & 271 \pm 4 & 0 \pm 2 \\ 0.1 \pm 0.6 & -0.8 \pm 1.5 & 256 \pm 4 \end{pmatrix}$$

$$\boldsymbol{\sigma}_{^{17}\mathrm{O}}^{\mathrm{B3LYP}}(4) = \begin{pmatrix} 289.7 \pm 1.0 & 0.1 \pm 0.6 & -0.1 \pm 0.5 \\ 0.1 \pm 0.6 & 261.1 \pm 0.9 & -0.3 \pm 0.4 \\ -0.2 \pm 0.3 & 0.0 \pm 0.4 & 253.1 \pm 0.8 \end{pmatrix}$$

$$\boldsymbol{\sigma}_{^{17}\mathrm{O}}^{\mathrm{B3LYP}}(5a) = \begin{pmatrix} 293 \pm 4 & 2 \pm 2 & 2.8 \pm 1.2 \\ 2.9 \pm 1.7 & 261 \pm 4 & -1 \pm 2 \\ 2.0 \pm 0.7 & -0.5 \pm 1.3 & 252 \pm 3 \end{pmatrix}$$

$$\boldsymbol{\sigma}_{^{17}\mathrm{O}}^{\mathrm{B3LYP}}(5d) = \begin{pmatrix} 288 \pm 3 & 1.7 \pm 1.4 & 0.5 \pm 0.8 \\ 2.0 \pm 1.2 & 262 \pm 2 & 1.0 \pm 0.8 \\ 0.5 \pm 0.4 & 0.3 \pm 0.8 & 253 \pm 2 \end{pmatrix}$$

$$\boldsymbol{\sigma}_{^{17}\mathrm{O}}^{\mathrm{B3LYP}}(6) = \begin{pmatrix} 280 \pm 6 & 3 \pm 6 & 1 \pm 3 \\ 2 \pm 6 & 246 \pm 3 & 5 \pm 4 \\ 1.6 \pm 1.1 & 4 \pm 2 & 247 \pm 4 \end{pmatrix}$$

$$\boldsymbol{\sigma}_{^{17}\mathrm{O}}^{\mathrm{B3LYP}}(l) = \begin{pmatrix} 290.7 \pm 0.8 & 0.3 \pm 0.5 & 0.0 \pm 0.4 \\ 0.7 \pm 0.5 & 261.7 \pm 0.8 & 0.0 \pm 0.4 \\ 0.1 \pm 0.2 & 0.1 \pm 0.4 & 253.2 \pm 0.7 \end{pmatrix}$$

Figure 7. Average ^{17}O nuclear magnetic shielding tensor (in ppm) for water in the liquid and gaseous states and for the various hydrogen-bonding species in the liquid at 300 K. The molecule is in the *xy* plane, with the C_2 axis in the *y* direction. The error limits for the 2-fold hydrogen-bonded species have been omitted because of the small size of the statistical sample.

$$\boldsymbol{\sigma}_{^{1}\mathrm{H}}^{\mathrm{B3LYP}}(g) = \begin{pmatrix} 36.93 \pm 0.07 & 7.72 \pm 0.04 & 0.00 \pm 0.00 \\ 5.43 \pm 0.05 & 29.57 \pm 0.07 & 0.00 \pm 0.00 \\ 0.00 \pm 0.00 & 0.00 \pm 0.00 & 23.70 \pm 0.03 \end{pmatrix}$$

$$\boldsymbol{\sigma}_{^{1}\mathrm{H}}^{\mathrm{B3LYP}}(2) = \begin{pmatrix} 35.5 & 10.3 & 0.7 \\ 9.0 & 26.7 & 0.6 \\ 1.1 & 0.8 & 19.5 \end{pmatrix}$$

$$\boldsymbol{\sigma}_{^{1}\mathrm{H}}^{\mathrm{B3LYP}}(3a0) = \begin{pmatrix} 35.8 \pm 0.7 & 6.7 \pm 0.4 & -0.11 \pm 0.15 \\ 5.9 \pm 0.5 & 29.9 \pm 0.7 & 0.0 \pm 0.5 \\ -0.1 \pm 0.3 & 0.3 \pm 0.5 & 23.3 \pm 0.9 \end{pmatrix}$$

$$\boldsymbol{\sigma}_{^{1}\mathrm{H}}^{\mathrm{B3LYP}}(3a1) = \begin{pmatrix} 32.2 \pm 1.2 & 14.5 \pm 1.0 & -0.3 \pm 0.5 \\ 13.2 \pm 1.0 & 24.8 \pm 1.3 & -0.1 \pm 0.9 \\ -0.2 \pm 0.6 & -0.1 \pm 0.9 & 11.4 \pm 1.3 \end{pmatrix}$$

$$\boldsymbol{\sigma}_{^{1}\mathrm{H}}^{\mathrm{B3LYP}}(3d) = \begin{pmatrix} 35.9 \pm 0.4 & 10.9 \pm 0.4 & 0.2 \pm 0.4 \\ 9.6 \pm 0.5 & 25.3 \pm 0.6 & 0.05 \pm 0.14 \\ 0.5 \pm 0.4 & 0.07 \pm 0.15 & 16.7 \pm 0.5 \end{pmatrix}$$

$$\boldsymbol{\sigma}_{^{1}\mathrm{H}}^{\mathrm{B3LYP}}(4) = \begin{pmatrix} 34.23 \pm 0.15 & 12.20 \pm 0.10 & -0.15 \pm 0.09 \\ 11.22 \pm 0.11 & 24.4 \pm 0.2 & -0.12 \pm 0.05 \\ -0.15 \pm 0.09 & -0.11 \pm 0.06 & 15.3 \pm 0.15 \end{pmatrix}$$

$$\boldsymbol{\sigma}_{^{1}\mathrm{H}}^{\mathrm{B3LYP}}(5a1) = \begin{pmatrix} 35.1 \pm 0.8 & 13.1 \pm 0.6 & 0.7 \pm 0.4 \\ 12.1 \pm 0.6 & 22.6 \pm 0.9 & 0.8 \pm 0.3 \\ 0.9 \pm 0.4 & 0.8 \pm 0.3 & 13.0 \pm 0.8 \end{pmatrix}$$

$$\boldsymbol{\sigma}_{^{1}\mathrm{H}}^{\mathrm{B3LYP}}(5a2) = \begin{pmatrix} 35.1 \pm 0.5 & 8.9 \pm 0.4 & 0.3 \pm 0.2 \\ 7.9 \pm 0.5 & 26.5 \pm 0.7 & -0.8 \pm 0.2 \\ 0.5 \pm 0.2 & -0.7 \pm 0.2 & 19.1 \pm 0.7 \end{pmatrix}$$

$$\boldsymbol{\sigma}_{^{1}\mathrm{H}}^{\mathrm{B3LYP}}(5d) = \begin{pmatrix} 33.6 \pm 0.3 & 12.5 \pm 0.3 & 0.18 \pm 0.13 \\ 11.5 \pm 0.3 & 25.0 \pm 0.4 & 0.01 \pm 0.13 \\ 0.31 \pm 0.15 & 0.04 \pm 0.14 & 15.4 \pm 0.4 \end{pmatrix}$$

$$\boldsymbol{\sigma}_{^{1}\mathrm{H}}^{\mathrm{B3LYP}}(6) = \begin{pmatrix} 34.5 \pm 0.6 & 10.0 \pm 0.5 & 1.0 \pm 0.3 \\ 9.0 \pm 0.5 & 23.9 \pm 0.7 & 0.55 \pm 0.15 \\ 1.2 \pm 0.3 & 0.64 \pm 0.14 & 17.1 \pm 1.2 \end{pmatrix}$$

$$\boldsymbol{\sigma}_{^{1}\mathrm{H}}^{\mathrm{B3LYP}}(l) = \begin{pmatrix} 34.30 \pm 0.12 & 12.02 \pm 0.09 & -0.01 \pm 0.06 \\ 11.02 \pm 0.10 & 24.60 \pm 0.14 & -0.07 \pm 0.05 \\ -0.03 \pm 0.07 & -0.05 \pm 0.05 & 15.49 \pm 0.13 \end{pmatrix}$$

Figure 8. As in Figure 7 but for the ^{1}H nuclear magnetic shielding tensor (in ppm).

weighted average of any tensor component yields the corresponding liquid-state tensor component. This is most easily seen with the diagonal components because they are relatively more precise than the off-diagonal components. It is interesting to note, for example, how the off-diagonal *xy* component in the plane of the molecule behaves. This component is negative in species *2* and increases with more hydrogen bonds, is zero in the liquid-like state (4-fold hydrogen-bonded case), and continues to grow toward positive values as the neighborhood becomes more crowded (5- and 6-fold hydrogen-bonded cases). The appearance of large off-diagonal components in the ^{17}O property tensors indicates significant deviation from the C_{2v} site symmetry for this nucleus for the hydrogen-bonding species in question. The similarities of the diagonal elements of the species with four or five hydrogen bonds are visible. The differences between the species occur in the behavior of the off-diagonal elements. These alterations are therefore more difficult to observe in NMR experiments.

In the hydrogen shielding tensors, the *xx* and *yy* components remain roughly constant, whereas the off-plane *zz* and off-diagonal, in-plane *xy* and *yx* components display the greatest variation with the local hydrogen-bonding pattern. The lack of the hydrogen bond (*3a0*) or, alternatively, an extra bond (*5a2*) at a hydrogen center causes the ^{1}H shielding tensor for this center to resemble the gas-state tensor more than those of the other species. The 2-fold hydrogen-bonding instances include two dramatically different cases from the point of view of the ^{1}H nucleus (whether or not the single existing hydrogen-bond acceptor bonds to the hydrogen atom with the nucleus in question), but our small statistical sample prevents us from presenting separate average tensors for the two cases. The ^{1}H shielding tensors of species *4* and the total liquid are again very similar.

3.4.2. Quadrupole Coupling Tensors for ^{17}O and ^{2}D. Figures 9 and 10 display the NQC tensors for ^{17}O and ^{2}D nuclei, respectively. The oxygen tensors are diagonal in the gaseous and liquid states. Also, the tensor for the case with four hydrogen bonds is almost diagonal within the error limits. The 2-fold hydrogen-bonded case and the *3d* instances have ^{17}O NQC tensors that are closest to the gaseous state, as expected. The progression of tensor components follows the above-presented discussion for the ^{17}O shielding constant. The *xx* and *zz* components are mostly affected by the hydrogen-bonding pattern. Configurations with a similar local situation at the oxygen site tend to have similar property tensors.

For deuterium, the situation is different. The most gas like species is *3a0*, in which the deuterium in question is not involved in a hydrogen bond. Most of its tensor components exceed even the gaseous values, as mentioned earlier. This reflects the effect of the presence of the acceptor at the other hydrogen center and the donors at the oxygen site.

$$\chi_{^{17}\mathrm{O}}^{\mathrm{B3LYP}}(g) = \begin{pmatrix} -8.88 \pm 0.04 & 0.00 \pm 0.02 & 0.00 \pm 0.00 \\ 0.00 \pm 0.02 & -1.87 \pm 0.05 & 0.00 \pm 0.00 \\ 0.00 \pm 0.00 & 0.00 \pm 0.00 & 10.75 \pm 0.03 \end{pmatrix}$$

$$\chi_{^{17}\mathrm{O}}^{\mathrm{B3LYP}}(2) = \begin{pmatrix} -7.6 & -1.1 & 0.2 \\ -1.1 & -1.4 & -0.7 \\ 0.2 & -0.7 & 9.0 \end{pmatrix}$$

$$\chi_{^{17}\mathrm{O}}^{\mathrm{B3LYP}}(3a) = \begin{pmatrix} -7.3 \pm 0.4 & 0.2 \pm 0.7 & 0.00 \pm 0.10 \\ 0.2 \pm 0.7 & -0.8 \pm 0.4 & -0.1 \pm 0.2 \\ 0.00 \pm 0.10 & -0.1 \pm 0.2 & 8.1 \pm 0.3 \end{pmatrix}$$

$$\chi_{^{17}\mathrm{O}}^{\mathrm{B3LYP}}(3d) = \begin{pmatrix} -7.5 \pm 0.2 & -0.24 \pm 0.12 & 0.03 \pm 0.06 \\ -0.24 \pm 0.12 & -1.14 \pm 0.15 & 0.0 \pm 0.2 \\ 0.03 \pm 0.06 & 0.0 \pm 0.2 & 8.61 \pm 0.15 \end{pmatrix}$$

$$\chi_{^{17}\mathrm{O}}^{\mathrm{B3LYP}}(4) = \begin{pmatrix} -6.89 \pm 0.05 & 0.07 \pm 0.05 & -0.05 \pm 0.02 \\ 0.07 \pm 0.05 & -0.77 \pm 0.05 & -0.03 \pm 0.03 \\ -0.05 \pm 0.02 & -0.03 \pm 0.03 & 7.66 \pm 0.05 \end{pmatrix}$$

$$\chi_{^{17}\mathrm{O}}^{\mathrm{B3LYP}}(5a) = \begin{pmatrix} -6.98 \pm 0.13 & 0.3 \pm 0.3 & 0.04 \pm 0.05 \\ 0.3 \pm 0.3 & -0.9 \pm 0.2 & 0.05 \pm 0.08 \\ 0.04 \pm 0.05 & 0.05 \pm 0.08 & 7.9 \pm 0.2 \end{pmatrix}$$

$$\chi_{^{17}\mathrm{O}}^{\mathrm{B3LYP}}(5d) = \begin{pmatrix} -6.86 \pm 0.11 & 0.15 \pm 0.10 & 0.01 \pm 0.04 \\ 0.15 \pm 0.10 & -0.92 \pm 0.09 & 0.06 \pm 0.07 \\ 0.01 \pm 0.04 & 0.06 \pm 0.07 & 7.78 \pm 0.11 \end{pmatrix}$$

$$\chi_{^{17}\mathrm{O}}^{\mathrm{B3LYP}}(6) = \begin{pmatrix} -7.1 \pm 0.2 & 0.4 \pm 0.4 & 0.05 \pm 0.07 \\ 0.4 \pm 0.4 & -1.1 \pm 0.3 & -0.08 \pm 0.11 \\ 0.05 \pm 0.07 & -0.08 \pm 0.11 & 8.2 \pm 0.3 \end{pmatrix}$$

$$\chi_{^{17}\mathrm{O}}^{\mathrm{B3LYP}}(l) = \begin{pmatrix} -6.94 \pm 0.05 & 0.08 \pm 0.05 & -0.02 \pm 0.02 \\ 0.08 \pm 0.05 & -0.83 \pm 0.05 & -0.01 \pm 0.03 \\ -0.02 \pm 0.02 & -0.01 \pm 0.03 & 7.77 \pm 0.05 \end{pmatrix}$$

Figure 9. As in Figure 7 but for the ^{17}O quadrupole coupling tensor (in MHz).

3.5. Anisotropic Properties. The shielding anisotropy and asymmetry parameters for both the shielding and the NQC tensors of ^{17}O and ^{1}H/^{2}D are gathered in Tables 1 and 2, respectively, for all hydrogen-bonding species along with the gaseous- and liquid-state values. These quantities are experimentally accessible only in anisotropic environments in static NMR spectra or, for example, via relaxation rates for bulk liquid water.[41] The data in the Tables corresponds to method 1 referred to in our previous work,[9] i.e., averaging the full tensor over the instantaneous configurations followed by diagonalization of the average tensor. However, the error limits are obtained by method 2, in which the diagonalization of instantaneous property tensors and the calculation of instantaneous anisotropic parameters precede the averaging of the latter. The error limits obtained from method 2 are not entirely compatible with the averages from method 1, but they serve as a qualitative indication of the magnitude of the statistical error.

In contrast to the corresponding shielding constants, the ^{17}O shielding anisotropy is notably different between species *3a* and *3d* and also between *5a* and *5d*. When the oxygen atom is not involved in two hydrogen bonds, the anisotropy is relatively close to the gaseous value, as seen with the *3d* species. Another systematic difference as compared to the behavior of the shielding constant occurs between species *4* and *5a*, in which the latter has a significantly larger shielding anisotropy. The shielding constants of the two cases are rather similar. The ^{1}H shielding anisotropies increase with the number of hydrogen bonds. The difference between the *3a0* and *3a1* species is large: the *3a0* value is close to the gaseous-state value, as expected. The *3a1* value is twice as large, being somewhat larger than the liquid-state value. The difference between the *5a1* and *5a2* species is also significant. The behavior of ^{1}H anisotropies follows the trend of ^{1}H shielding constants.

$$\chi_{^{2}\mathrm{D}}^{\mathrm{B3LYP}}(g) = \begin{pmatrix} 119.6 \pm 1.4 & 166 \pm 3 & 0.0 \pm 0.0 \\ 166 \pm 3 & 20.4 \pm 0.7 & 0.0 \pm 0.0 \\ 0.0 \pm 0.0 & 0.0 \pm 0.0 & -139.8 \pm 1.4 \end{pmatrix}$$

$$\chi_{^{2}\mathrm{D}}^{\mathrm{B3LYP}}(2) = \begin{pmatrix} 110.9 & 152.9 & -0.5 \\ 152.9 & 18.4 & 0.6 \\ -0.5 & 0.6 & -129.3 \end{pmatrix}$$

$$\chi_{^{2}\mathrm{D}}^{\mathrm{B3LYP}}(3a0) = \begin{pmatrix} 126 \pm 13 & 175 \pm 11 & -0.4 \pm 0.5 \\ 175 \pm 11 & 14 \pm 7 & 1.2 \pm 0.6 \\ -0.4 \pm 0.5 & 1.2 \pm 0.6 & -141 \pm 9 \end{pmatrix}$$

$$\chi_{^{2}\mathrm{D}}^{\mathrm{B3LYP}}(3a1) = \begin{pmatrix} 83 \pm 7 & 110 \pm 8 & 0.3 \pm 0.8 \\ 110 \pm 8 & 12 \pm 4 & 1.7 \pm 1.4 \\ 0.3 \pm 0.8 & 1.7 \pm 1.4 & -95 \pm 6 \end{pmatrix}$$

$$\chi_{^{2}\mathrm{D}}^{\mathrm{B3LYP}}(3d) = \begin{pmatrix} 99 \pm 4 & 134 \pm 6 & 0.0 \pm 0.6 \\ 134 \pm 6 & 14 \pm 2 & 0.2 \pm 0.5 \\ 0.0 \pm 0.6 & 0.2 \pm 0.5 & -113 \pm 4 \end{pmatrix}$$

$$\chi_{^{2}\mathrm{D}}^{\mathrm{B3LYP}}(4) = \begin{pmatrix} 90.8 \pm 1.1 & 124.0 \pm 1.3 & 0.7 \pm 0.2 \\ 124.0 \pm 1.3 & 12.2 \pm 0.6 & -0.09 \pm 0.14 \\ 0.7 \pm 0.2 & -0.09 \pm 0.14 & -103.0 \pm 1.0 \end{pmatrix}$$

$$\chi_{^{2}\mathrm{D}}^{\mathrm{B3LYP}}(5a1) = \begin{pmatrix} 87 \pm 6 & 122 \pm 10 & -0.4 \pm 0.9 \\ 122 \pm 10 & 14 \pm 3 & -0.2 \pm 0.5 \\ -0.4 \pm 0.9 & -0.2 \pm 0.5 & -102 \pm 7 \end{pmatrix}$$

$$\chi_{^{2}\mathrm{D}}^{\mathrm{B3LYP}}(5a2) = \begin{pmatrix} 105 \pm 5 & 145 \pm 6 & -1.0 \pm 0.6 \\ 145 \pm 6 & 13 \pm 3 & 0.4 \pm 0.5 \\ -1.0 \pm 0.6 & 0.4 \pm 0.5 & -118 \pm 5 \end{pmatrix}$$

$$\chi_{^{2}\mathrm{D}}^{\mathrm{B3LYP}}(5d) = \begin{pmatrix} 90 \pm 3 & 124 \pm 3 & -0.1 \pm 0.4 \\ 124 \pm 3 & 13.2 \pm 1.1 & -0.3 \pm 0.4 \\ -0.1 \pm 0.4 & -0.3 \pm 0.4 & -103 \pm 3 \end{pmatrix}$$

$$\chi_{^{2}\mathrm{D}}^{\mathrm{B3LYP}}(6) = \begin{pmatrix} 91 \pm 5 & 130 \pm 5 & -0.4 \pm 1.3 \\ 130 \pm 5 & 14 \pm 4 & -0.8 \pm 1.0 \\ -0.4 \pm 1.3 & -0.8 \pm 1.0 & -105 \pm 4 \end{pmatrix}$$

$$\chi_{^{2}\mathrm{D}}^{\mathrm{B3LYP}}(l) = \begin{pmatrix} 91.8 \pm 1.0 & 125.7 \pm 1.4 & -0.3 \pm 0.3 \\ 125.7 \pm 1.4 & 12.6 \pm 0.5 & -0.07 \pm 0.14 \\ -0.3 \pm 0.3 & -0.07 \pm 0.14 & -104.4 \pm 0.9 \end{pmatrix}$$

Figure 10. As in Figure 7 but for the ^{2}D quadrupole coupling tensor (in kHz).

4. Conclusions

Molecules in the liquid state are surrounded by a dynamically changing environment. In this work, a Car−Parrinello molecular dynamics simulation trajectory of liquid water is sampled by quantum-chemical NMR property calculations and used to divide the liquid-state water molecules into distinct species that differ in the number of hydrogen bonds in which they are engaged. Full average tensors for nuclear magnetic shielding and quadrupole coupling and the various NMR parameters derived from these tensors are reported for different 2-, 3-, 4-, 5-, and 6-fold hydrogen-bonded instantaneous water species. The total liquid-state parameters are the weighted averages of the parameters of these classes. We also report the distributions of the individual property values among each species.

The results show how the interaction with the environment, including thermal averaging due to simulation, affects the NMR parameters. Whereas systematic changes in the average NMR parameters occur as a function of the number of hydrogen bonds,

the distributions of the parameters in the instantaneous configurations overlap between the different hydrogen-bonding species. This is likely to make addressing the question of the average hydrogen bond number in liquid water difficult by NMR techniques.

A broken or extra hydrogen bond induces major changes in the NMR parameters. This is seen by comparing the two nonequivalent hydrogen nuclei within species that have either three or five hydrogen bonds. Compared to the 4-fold hydrogen-bonded case, the absence of the bond or an excess bond shifts the values closer to the gas-state value. For hydrogen/deuterium, the effect is much more pronounced than it is for oxygen. It is found that two nearby oxygens for one hydrogen make the NMR parameters of the latter more gas like, reflecting weak hydrogen bonding associated with large bond lengths.

In the present data, completely nonoverlapping property distributions between differently hydrogen-bonded species, with a significant population of the species in the underlying Car−Parrinello simulation, occur only for the ^{1}H shielding and the ^{2}D quadrupole coupling constants in the 3-fold hydrogen-bonded instances, in which the resonating nucleus either is or is not involved in a hydrogen bond to an acceptor molecule. In the case of ^{17}O parameters, the fact that the behavior of the anisotropic shielding as a function of the number of hydrogen bonds is different from the isotropic shielding constant could turn out to be useful in designing NMR experiments.

The criterion used in classifying the instantaneous configurations into different hydrogen-bonding species is a matter of choice and may somewhat influence the conclusions reached. Presently, we employ a simple and robust one-parameter distance criterion. An investigation of the consequences of different choices is in progress in our laboratory.

Acknowledgment. Professors Jukka Jokisaari and Kari Laasonen (Oulu, Finland) are acknowledged for fruitful discussions and collaboration in the initial phases of this work. We are grateful for the financial support from the Finnish Cultural Foundation (T.S.P.) and the Emil Aaltonen Foundation (J.V.). T.S.P., P.L., and J.V. belong to the Finnish Center of Excellence in Computational Molecular Science (CMS, 2006-11). J.V. is an Academy Research Fellow of the Academy of Finland. Computational resources were partially provided by CSC - Scientific Computing Ltd., Espoo, Finland. The DFT calculations were carried out with Dalton prerelease version 2.0, kindly placed at our disposal by T. Helgaker and P. Sałek.

References and Notes

(1) Helgaker, T.; Jaszuński, M.; Ruud, K. *Chem. Rev.* **1999**, *99*, 293.
(2) Mikkelsen, K. V.; Ruud, K.; Helgaker, T. *Chem. Phys. Lett.* **1996**, *253*, 443.
(3) Searles, D. B.; Huber, H. In *Encyclopedia of Nuclear Magnetic Resonance;* Grant, D. M., Harris, R. K., Eds.; Wiley & Sons: Chichester, 2002; Vol. 9.
(4) Cossi, M.; Crescenzi, O. *J. Chem. Phys.* **2003**, *118*, 8863.
(5) Malkin, V. G.; Malkina, O. L.; Steinebrunner, G.; Huber, H. *Chem.−Eur. J.* **1996**, *2*, 452.
(6) Sebastiani, D.; Parrinello, M. *J. Phys. Chem. A* **2001**, *105*, 1951.
(7) Mauri, F.; Pfrommer, B. G.; Louie, S. G. *Phys. Rev. Lett.* **1996**, *77*, 5300.
(8) Car, R.; Parrinello, M. *Phys. Rev. Lett.* **1985**, *55*, 2471.
(9) Pennanen, T. S.; Vaara, J.; Lantto, P.; Sillanpää, A. J.; Laasonen, K.; Jokisaari, J. *J. Am. Chem. Soc.* **2004**, *126*, 11093.
(10) Eckart, C. *Phys. Rev.* **1935**, *47*, 552.
(11) Vaara, J.; Lounila, J.; Ruud, K.; Helgaker, T. *J. Chem. Phys.* **1998**, *109*, 8388.
(12) Wernet, Ph.; Nordlund, D.; Bergmann, U.; Cavalleri, M.; Odelius, M.; Ogasawara, H.; Näslund, L. Å.; Hirsch, T. K.; Ojamäe, L.; Glatzel, P.; Pettersson, L. G. M.; Nilsson, A. *Science* **2004**, *304*, 995.
(13) Smith, J. D.; Cappa, C. D.; Wilson, K. R.; Messer, B. M.; Cohen, R. C.; Saykally, R. J. *Science* **2004**, *306*, 851.
(14) Mantz, Y. A.; Chen, B.; Martyna, G. J. *Chem. Phys. Lett.* **2005**, *405*, 294.
(15) Nilsson, A.; Wernet, Ph.; Nordlund, D.; Bergmann, U.; Cavalleri, M.; Odelius, M.; Ogasawara, H.; Näslund, L. Å.; Hirsch, T. K.; Ojamäe, L.; Glatzel, P.; Pettersson, L. G. M. *Science* **2005**, *308*, 793a.
(16) Smith, J. D.; Cappa, C. D.; Messer, B. M.; Cohen, R. C.; Saykally, R. J. *Science* **2005**, *308*, 793b.
(17) See, for example, Modig, K.; Pfrommer, B. G.; Halle, B. *Phys. Rev. Lett.* **2003**, *90*, 075502.
(18) Klein, R. A.; Mennucci, B.; Tomasi, J. *J. Phys. Chem. A* **2004**, *108*, 5851.
(19) Cybulski, H.; Sadlej, J. *Chem. Phys.* **2006**, *323*, 218.
(20) The simulations have been performed with the FINGER program, which has mainly been developed at the Helsinki University of Technology, Espoo, Finland. It is based largely on techniques presented in the paper by Laasonen, K.; Pasquarello, A.; Car, R.; Lee, C.; Vanderbilt, D. *Phys. Rev. B* **1993**, *47*, 10142.
(21) Becke, A. D. *Phys. Rev. A* **1988**, *38*, 3098. Lee, C.; Yang, W.; Parr, R. *Phys. Rev. B* **1988**, *37*, 785.
(22) Vanderbilt, D. *Phys. Rev. B* **1990**, *41*, 5048. Laasonen, K.; Car, R.; Lee, C.; Vanderbilt, D. *Phys. Rev. B* **1991**, *43*, 6796.
(23) Helgaker, T.; Jensen, H. J. Aa.; Jørgensen, P.; Olsen, J.; Ruud, K.; Ågren, H.; Bak, K. L.; Bakken, V.; Christiansen, O.; Coriani, S.; Dahle, P.; Dalskov, E. K.; Enevoldsen, T.; Fernandez, B.; Hættig, C.; Hald, K.; Halkier, A.; Heiberg, H.; Hettema, H.; Jonsson, D.; Kirpekar, S.; Kobayashi, R.; Koch, H.; Mikkelsen, K. V.; Norman, P.; Packer, M. J.; Ruden, T. A.; Saue, T.; Sauer, S. P. A.; Schimmelpfennig, B.; Sylvester-Hvid, K. O.; Taylor, P. R.; Vahtras, O. *Dalton*, release 1.2 (2001), an electronic structure program. See http://www.kjemi.uio.no/software/dalton/dalton.html.
(24) Becke, A. D. *J. Chem. Phys.* **1993**, *98*, 5648. Stephens, P. J.; Devlin, F. J.; Chabalowski, C. F.; Frisch, M. J. *J. Phys. Chem.* **1994**, *98*, 11623.
(25) Cheeseman, J. R.; Trucks, G. W.; Keith, T. A.; Frisch, M. J. *J. Chem. Phys.* **1996**, *104*, 5497.
(26) Helgaker, T.; Wilson, P. J.; Amos, R. D.; Handy, N. C. *J. Chem. Phys.* **2000**, *113*, 2983.
(27) Magyarfalvi, G.; Pulay, P. *J. Chem. Phys.* **2003**, *119*, 1350.
(28) Chesnut, D. B. *Chem. Phys. Lett.* **2003**, *380*, 251.
(29) Dunning, T., Jr. *J. Chem. Phys.* **1989**, *90*, 1007.
(30) Mikkelsen, K.; Jørgensen, P.; Ruud, K.; Helgaker, T. *J. Chem. Phys.* **1997**, *106*, 1170.
(31) Stillinger, F. H. *Science* **1980**, *209*, 451.
(32) Jorgensen, W. L.; Chandrasekhar, J.; Madura, J. D.; Impey, R. W.; Klein, M. L. *J. Chem. Phys.* **1983**, *79*, 926.
(33) Mezei, M.; Beveridge, D. L. *J. Chem. Phys.* **1981**, *74*, 622.
(34) Kuo, I. W.; Mundy, C. J. *Science* **2004**, *303*, 658.
(35) Florin, A.; Alei, M., Jr. *J. Chem. Phys.* **1967**, *47*, 4268.
(36) Raynes, W. T. *Mol. Phys.* **1983**, *49*, 443.
(37) Sebastiani, D.; Parrinello, M. *Chem. Phys. Chem.* **2002**, *3*, 675.
(38) Hindman, J. C. *J. Chem. Phys.* **1966**, *44*, 4582.
(39) Raynes, W. T. In *Nuclear Magnetic Resonance, A Specialist Periodical Report*, Royal Society of Chemistry: London, 1978; Vol. 7, p 1.
(40) Eggenberger, R.; Gerber, S.; Huber, H.; Searles, D.; Welker, M. *J. Chem. Phys.* **1992**, *97*, 5898.
(41) Modig, K.; Halle, B. *J. Am. Chem. Soc.* **2002**, *124*, 12031.